Inorganic Chemistry
Article
Cite This: Inorg. Chem. XXXX, XXX, XXX−XXX
pubs.acs.org/IC

Highly Active $Mn_{3-x}Fe_xO_4$ Spinel with Defects for Toluene Mineralization: Insights into Regulation of the Oxygen Vacancy and Active Metals

Lizhong Liu,*[,†] Jiangtian Sun,[‡] Jiandong Ding,[†] Yan Zhang,[†] Tonghua Sun,*[,§] and Jinping Jia[§]

[†]School of Chemistry and Chemical Engineering, Nantong University, 9 Seyuan Road, Nantong 226019, Jiangsu Province,P. R. China

[‡]Department of Chemistry, Xi'an Jiaotong-Liverpool University, 111 Ren'ai Road, Suzhou Dushu Lake Science and Education Innovation District, Suzhou Industrial Park, Suzhou 215123, P. R. China

[§]School of Environmental Science and Engineering, Shanghai Jiao Tong University, 800 Dong Chuan Road, Shanghai 200240, P. R. China

Supporting Information

ABSTRACT: A series of highly defected $Mn_{3-x}Fe_xO_4$ spinels with different amounts of oxygen vacancies and active metals were successfully synthesized by regulating the insertion of Fe ions into the crystal structure of Mn_3O_4 via self-polymerizable monomer adjustment of the molten Mn−Fe salt dispersion. The characterization of X-ray diffraction, Raman, scanning electron microscopy, X-ray photoelectron spectroscopy, and N_2 adsorption−desorption showed that the doping of Fe increased the lattice defects, oxygen vacancy concentration, specific surface area, mesoporosity, and catalytic properties compared to Cu ions doping. Temperature-programmed reduction with hydrogen and oxygen pulse chemisorption tests determined that the doping level of Fe ions had an important influence on the oxygen vacancy content and the dispersion of active metals on the catalysts' surfaces. For the best Mn-dispersed and most active $Mn_{2.4}Fe_{0.6}O_4$ catalyst, a long-term toluene oxidation measurement running for 120 h of uninterrupted reaction, at the low temperature of 240 °C, high humidity (relative humidity = 100%), and high weight hourly space velocity of 60000 $mL·g^{-1}·h^{-1}$, was also carried out, which indicated that the catalyst possessed high stability and endurability. Moreover, the continuous oxidation route and internal principle for toluene oxidation were also revealed by the in situ diffuse-reflectance infrared Fourier transform spectroscopy and gas chromatography−mass spectrometry techniques and deep dynamics study.

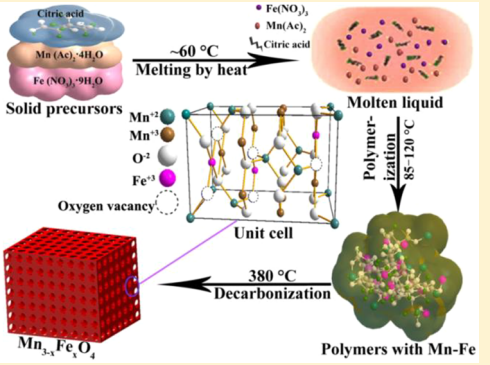

1. INTRODUCTION

Volatile organic compounds (VOCs), as precursors of photochemical smog and ozone, are attracting wide attention because of their toxic, mutagenic, carcinogenic, and teratogenetic nature.[1−3] Among various VOCs, toluene, as one of the 189 harmful air pollutants indicated in CAAA90, is a typical gaseous pollutant that is relatively difficult to remove at low temperature because of its chemical stability.[4−6] At present, various control technologies, such as photodegradation,[7] biodegradation,[8] physical separation,[9] plasma oxidation,[10] and catalytic oxidation,[11] have been developed for toluene removal, and catalytic oxidation is recognized as the best economical and efficient technology because it can convert toluene to carbon dioxide (CO_2) and water (H_2O) at relatively low temperature.[12,13] As is known, the key of catalytic oxidation is catalysts, which commonly include noble metals and transition-metal oxides.[14−16] Noble metals possess high catalytic activity, but their expense, sintering, coke, etc., limit their widespread use in VOC oxidation.[11,17−19] Therefore, many researchers are currently paying close attention to studies on transition-metal oxides.[18,20−22]

Spinel catalysts with AB_2O_4 structure, as one of the potential substitutes for noble metals, has received extensive attention in the removal of VOCs because of its polyvalence, affordability, and low toxicity.[23−29] It has been reported that heteroatom-doped spinels can create plenty of oxygen defects, which could improve performance because they can be used as reaction centers for the migration and complementation of oxygen species. Hammiche-Bellal et al.[30] prepared a $CoFe_2O_4$ composite spinel above 500 °C by a coprecipitation method, achieving good removal of ethanol. Behar et al.[31] studied the $Cu_{1.5}Mn_{1.5}O_4$ composite spinel for toluene oxidation, displaying high removal efficiency (RE). Castaño et al.[32] investigated the doped spinel $MnMgAlO_x$ catalyst for toluene removal, obtaining increased catalytic activity. However, it should be inappropriate to attribute the high activity of spinels to

Received: July 14, 2019

DOI: 10.1021/acs.inorgchem.9b02105
Inorg. Chem. XXXX, XXX, XXX−XXX

heteroatom doping while ignoring how doped heteroatoms affect its catalytic activity. Besides, the conventional syntheses of spinel catalysts must be a multistep independent manipulation, which is also distinctly relatively time-consuming and requires harsh conditions.

We herein first reported a facile and scalable method to synthesize a highly active heteroatom-doped spinel catalyst ($Mn_{3-x}Fe_xO_4$) at relatively low temperature. Regulation of the oxygen vacancy induction and dispersion of active metals were adjusted by controlling the ratio of precursors in molten metal salts. Combined with various characterizations, the influence of the doping ion type and degree on the microstructure and performance of the catalysts was investigatived in depth, and the important intrinsic link between the structure and catalytic behavior was revealed. Ultimately, the effects of the Fe doping amount on the catalytic performance and the long-term catalytic oxidation evaluation of toluene on the preferred active catalyst under simulated realistic exhaust conditions were also explored.

2. EXPERIMENTAL SECTION

2.1. Preparation of Catalysts. A series of $Mn_{3-x}Fe_xO_4$ (x = 0.5, 0.6, 0.7, and 1.0) catalysts were synthesized by a one-step heat treatment and are shown in Figure 1. The typical preparation

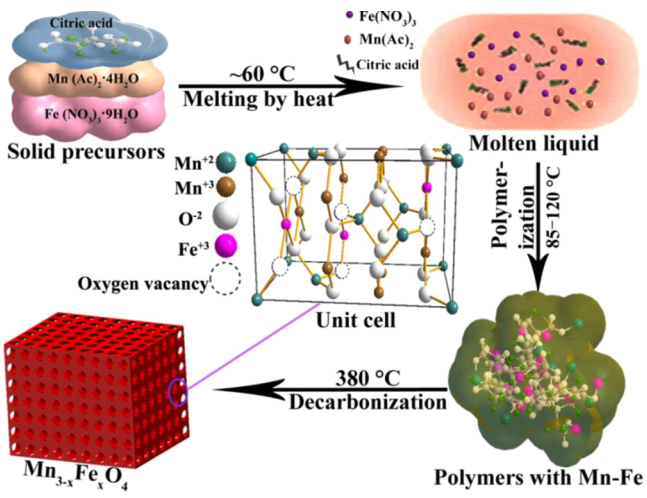

Figure 1. Representation of the $Mn_{3-x}Fe_xO_3$ spinels.

procedure of $Mn_{2.4}Fe_{0.6}O_4$ is as follows: 2.00 g of $Fe(NO_3)_3{\cdot}9H_2O$, 4.90 g of $Mn(CH_3COO)_2{\cdot}4H_2O$, and 7.88 g of citric acid were mingled; afterward, the above mingled system was heated up to 380 °C at 2 °C·min^{-1} and kept there for 2 h in a muffle furnace, which was placed in a fume hood with exhaust gas absorption. For comparison, $Fe(NO_3)_3{\cdot}9H_2O$ was replaced with 1.21 g of $Cu(NO_3)_3{\cdot}3H_2O$ to obtain $Mn_{3-x}Cu_xO_4$, and the amounts of $Mn(CH_3COO)_2{\cdot}4H_2O$ and citric acid were projected to be 4.90 and 6.30 g to obtain Mn_3O_4, and the sample obtained after removal of $Mn(Ac)_2{\cdot}4H_2O$ was γ-Fe_2O_3. The vendor details are provided in section S1.

2.2. Catalytic Evaluation. The catalytic activities of the catalysts for toluene oxidation were tested in a continuous-flow fixed-bed quartz microreactor (i.d. = 6.0 mm). A 100 mg sample was employed to assess the performance. The air stream, containing 1000 ppm of toluene and saturated steam produced by airblowing, passed through the sample layer at 100 mL·min^{-1} to obtain a weight hourly space velocity (WHSV) of 60000 mL·g^{-1}·h^{-1}. The moisture in the catalytic system was adjusted [relative humidity (RH) = 0, 55, and 100%] to measure the influence of steam on the performance. The RE and mineralization efficiency (ME) of toluene and apparent activation energy (E_a, kJ·mol^{-1}) for toluene mineralization were calculated byeqs 1−4

$$RE = \frac{[C_7H_8]_{in} - [C_7H_8]_{out}}{[C_7H_8]_{in}} \times 100\% \quad (1)$$

$$ME = \frac{[CO_2]_{out} - [CO_2]_{in}}{7[C_7H_8]_{in}} \times 100\% \quad (2)$$

$$r = \frac{[C_7H_8]_{in} Q ME}{m_{cat}} \quad (3)$$

$$E_a = -R \frac{d(\ln k)}{d\left(\frac{1}{T}\right)} \quad (4)$$

where $[C_7H_8]_{in}$, $[C_7H_8]_{out}$, $[CO_2]_{in}$, and $[CO_2]_{out}$ named the inlet and outlet concentrations of toluene and CO_2 (mol·mL^{-3}); r, Q, k, R, and T are the reaction rate (mol·g^{-1}·s^{-1}), volumetric flow (mL·s^{-1}), rate constant (mL·g^{-1}·s^{-1}), molar gas constant, and reaction temperature (K), respectively.

3. RESULTS AND DISCUSSION

Figure 2a shows the X-ray diffraction (XRD) results for both the doped and undoped spinels. The diffraction peaks of all

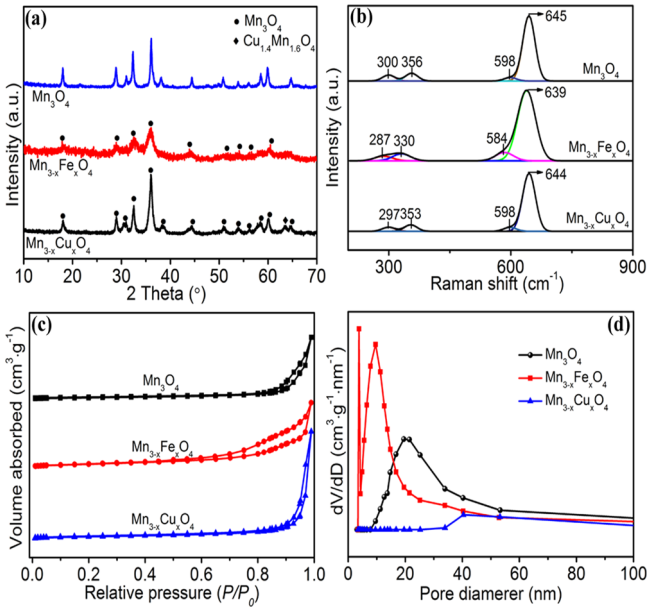

Figure 2. (a) XRD patterns, (b) Raman spectra, (c) N_2 adsorption−desorption isotherms, and (d) pore-size distributions of Mn_3O_4, $Mn_{3-x}Cu_xO_4$, and $Mn_{3-x}Fe_xO_4$ (x = 0.6).

catalysts according to that of the spinel Mn_3O_4 (JCPDS 18-0803) could be identifiable, indicating that the $Mn_{3-x}Cu_xO_4$ and $Mn_{3-x}Fe_xO_4$ samples showed crystalline structures similar to that of Mn_3O_4. After the adjunction of Fe and Cu to the synthesis system, the crystal growth of the original Mn_3O_4 obviously became disturbed and the diffraction peaks of new samples were broader compared to Mn_3O_4, which is attributed to the structural damage due to anisotropic expansion and contraction of the unit cell parameters,[33] suggesting that Fe and Cu ions can get into the framework of Mn_3O_4 and take over the sites of Mn during the crystal growth process, thus leading to crystalline defects being introduced to the catalyst, which helped to generate more oxygen vacancies. Besides, it should be noted that the sample doped with Cu also displayed

DOI: 10.1021/acs.inorgchem.9b02105
Inorg. Chem. XXXX, XXX, XXX−XXX

Table 1. Element Compositions, Surface Areas, and Peak Areas of Raman Spectra at 584−598 cm^{-1} of Catalysts

	feed (molar ratio)	XPS (molar ratio)				
sample (x = 0.6)	Mn/Fe (Cu)	Mn/Fe (Cu)	O_{ads}/O_{latt}	$(Mn^{3+} + Mn^{2+})/Mn^{4+}$	S_{BET} ($m^2 \cdot g^{-1}$)	peak area[a]
Mn_3O_4	0	0	0.47	1.88	23.4	690.2
$Mn_{3-x}Fe_xO_4$	4.00	4.16	0.89	2.33	84.8	1630.6
$Mn_{3-x}Cu_xO_4$	4.00	5.12	0.53	2.04	28.9	840.1

[a]Comprehensive area of the peak at 584−598 cm^{-1} over Raman spectra.

some traces of $Cu_{1.4}Mn_{1.6}O_4$ (JCPDS 35-1030), while the sample doped with Fe displayed no clear evidence for the formation of other types of metal oxides. This behavior may be interpreted by the ionic radius. The radius of Fe^{3+} (0.55 Å) is lower than that of Mn^{3+} (0.58 Å), which allowed the incorporation of Fe^{3+} in the Mn^{3+} sites of Mn_3O_4.[31] Nevertheless, the ionic radius of Cu^{2+} (0.73 Å) was higher than that (0.67 Å) of Mn^{2+},[34] impeding the incorporation of Cu^{2+} in the Mn^{2+} sites of Mn_3O_4, keeping Cu^{2+} from entering into the Mn_3O_4 crystals but causing it to bind to Mn^{3+} to form another crystal structure ($Cu_{1.4}Mn_{1.6}O_4$). Additionally, it can be found from Figure S4 that the X-ray photoelectron spectroscopy (XPS) characteristic peak of Cu appeared at 943.7 eV attributed to Cu^{3+},[35] demonstrating the existence of trivalent Cu. Indeed, many researchers have reported the existence of Cu^{3+} species in some solid oxides such as $La_{2-x}Sr_xCuO_4$,[36] La_2CuO_4,[37] Bi−Sr−Ca−Cu−O oxides,[38] $YBa_2Cu_3O_{6+y}$,[39] and Cu/Al_2O_3,[40] wherein Cu^{3+} was found. Su et al.[39] proposed the following transport behaviors of Cu ions under suitable conditions (eqs 5 and 6).

$$2Cu^{2+} \Leftrightarrow Cu^{+} + Cu^{3+} \quad (5)$$

$$Cu^{+} + \frac{1}{2}O_2 \Leftrightarrow O^{=} + Cu^{3+} \quad (6)$$

The degree of Cu^{2+} disproportionation was temperature-dependent, and Cu^{3+} increases with increasing O_2 content. Similarly, the above transport behaviors should also exist in our preparation system of Cu−Mn oxide, causing the presence of Cu^{3+}, which is inserted into the Mn_3O_4 lattice because of the lower ionic radius of Cu^{3+} compared to that of Mn^{3+}. Obviously, the Fe ions are more easily inserted into Mn_3O_4 than Cu ions, thus creating more surface defects for the catalyst.

The vibrational behavior of the lattices and structural divergence of three samples were analyzed by Raman spectroscopy, and all peaks of the samples were deconvoluted by the Gaussian method (Figure 2b).[41] For pure Mn_3O_4, four broad peaks are clearly presented: the T_{2g} symmetry modes at 300 and 598 cm^{-1}, the E_g symmetry mode at 356 cm^{-1}, and the A_{1g} symmetry "breathing" mode at 645 cm^{-1}.[42] With the addtion of Fe and Cu, the peaks for the $T_{2g}(1)$, E_g, and A_{1g} symmetry modes all showed negative shifts to some extent, hinting that the existence of crystal defects is due to the insertion of Fe and Cu into the Mn_3O_4 lattice through the partial substitution of Mn ions.[18,43,44] The oxygen vacancy concentration can be indirectly tested in the region of 584−598 cm^{-1}.[27,41] The corresponding peak areas are shown in Table 1, and the oxygen vacancy concentrations were in the order of $Mn_{3-x}Fe_xO_4$ > $Mn_{3-x}Cu_xO_4$ > Mn_3O_4. The increased defective sites facilitated the catalytic oxidation of toluene because they serve as reaction centers wherein the reactive species can be migrated and supplemented over oxygen vacancies. The results are consistent with those of XRD.

N_2 adsorption−desorption isotherms and pore-size distributions of $Mn_{3-x}Fe_xO_4$, $Mn_{3-x}Cu_xO_4$, and Mn_3O_4 are displayed in Figure 2c,d. As shown in Figure 2c, the isotherms of the catalysts showed a typical IUPAC type IV pattern, which is representative of a mesoporous material.[34,45,46] Figure 2d shows that the pore-size distributions were from 2 to 50 nm, confirming the presence of mesopores. Moreover, the Brunauer−Emmett−Teller (BET) surface areas of $Mn_{3-x}Fe_xO_4$, $Mn_{3-x}Cu_xO_4$, and Mn_3O_4 were 84.8, 28.9, and 23.4 $m^2 \cdot g^{-1}$ (Table 1), respectively. It is obvious that the addition of Fe led to a larger surface area, which should be attributed to the formation of more mesoporous structures on the catalyst surface, increasing the capacity of the catalytic oxidation of toluene.[47] Meanwhile, generated $Cu_{1.4}Mn_{1.6}O_4$ may have filled most of the mesopores, which weakened the number of mesopores in the catalysts and resulted in the insertion of Cu not significantly advancing the surface areas of the samples.

The scanning electron microscopy (SEM) images of three samples are displayed in Figure 3. From Figure 3a,b, it can be obviously seen that there is a large amount of irregular porosity in the wrinkled Mn_3O_4 catalyst. After Fe ion incorporation (Figure 3c,d), a large number of relatively ordered mesopores with a pore size of 19 ± 5 nm appeared in the catalyst ($Mn_{3-x}Fe_xO_4$), which greatly improved its specific surface area. The porous structure and high surface area are important to advancing the activity of the catalyst. This was conducive to the proximity of toluene molecules to catalysts.[45,48] However, the addition of Cu ions completely changed the original morphology of Mn_3O_4, and the SEM images of $Mn_{3-x}Cu_xO_4$ showed spheroidal nanoparticles, which may result in an insignificant rise in the surface area of the catalyst (Figure 3e,f). Analysis of the SEM images was consistent with that of the N_2 adsorption−desorption isotherms of the catalysts.

The Mn $2p_{3/2}$ and O 1s XPS spectra of Mn_3O_4, $Mn_{3-x}Fe_xO_4$, and $Mn_{3-x}Cu_xO_4$ are presented in Figure 4a,b. The molar ratio of the surface Mn/Fe for $Mn_{3-x}Fe_xO_4$ was 4.16, which was very close to that of the feed (Mn/Fe = 4/1), indicating that Fe ions were uniformly doped into Mn_3O_4. However, the molar ratio of the surface Mn/Cu (5.12) for $Mn_{3-x}Cu_xO_4$ was much higher than the feed molar ratio of Mn/Cu (4/1), showing that some Cu was not incorporated into Mn_3O_4. As shown in Figure 4a, the three components divided from the XPS spectrum of Mn $2p_{3/2}$ at 643.1, 641.9, and 640.7 eV correspond to the surface Mn^{4+}, Mn^{3+}, and Mn^{2+}, respectively.[48] The surface molar ratios of (Mn^{2+} + Mn^{3+}) to Mn^{4+} for $Mn_{3-x}Fe_xO_4$ (2.33) and $Mn_{3-x}Cu_xO_4$ (2.04) were higher than that of Mn_3O_4 (1.88), suggesting that the doped Fe and Cu ions can result in an increase of the surface Mn^{2+} and Mn^{3+}. The generation of oxygen vacancies (denoted as Δ) can be on the basis of eqs 7 and 8.[49] Namely, the presence of more low-valent Mn facilitates the appearance of more crystalline defects and oxygen vacancies in the catalysts, thus accelerating the process of converting O_2 to activated oxygen

DOI: 10.1021/acs.inorgchem.9b02105
Inorg. Chem. XXXX, XXX, XXX−XXX

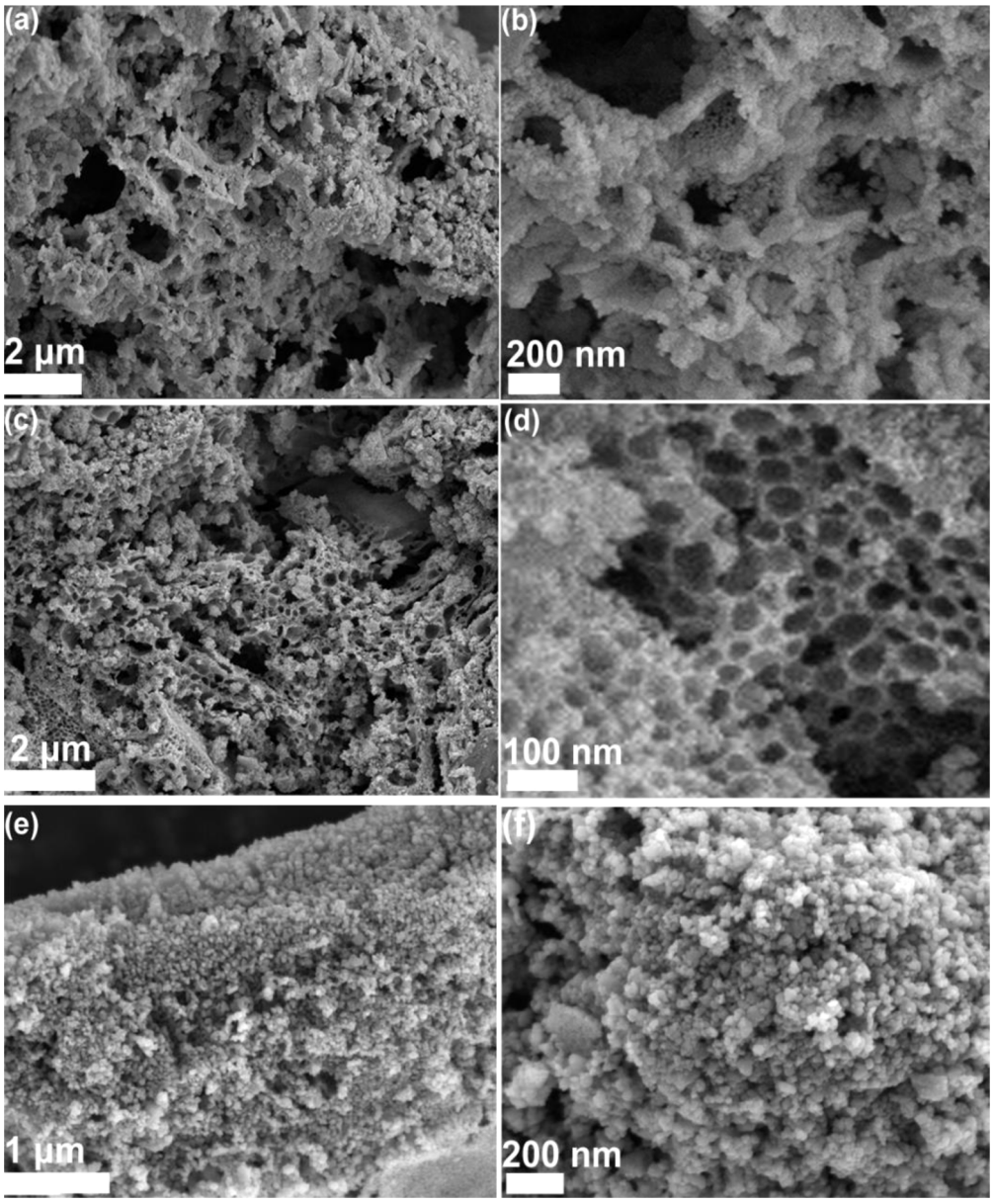

Figure 3. SEM images of (a and b) Mn_3O_4, (c and d) $Mn_{3-x}Cu_xO_4$, and (e,f) $Mn_{3-x}Fe_xO_4$ (x = 0.6).

species.[24,50] Besides, the surface molar ratio of (Mn^{2+} + Mn^{3+})/Mn^{4+} in $Mn_{3-x}Fe_xO_4$ was also much higher than that of $Mn_{3-x}Cu_xO_4$. This may be ascribed to the fact that Fe^{3+} ions have a greater chance of being inserted into the unit cell of Mn_3O_4 compared to Cu^{3+} because of the relatively difficult conversion of Cu^{2+} to Cu^{3+}.

$$Mn^{4+} - O^{2-} - Mn^{4+} \rightarrow Mn^{3+} - \Delta - Mn^{3+} + \frac{1}{2}O_2\uparrow \quad (7)$$

$$Mn^{3+} - O^{2-} - Mn^{3+} \rightarrow Mn^{2+} - \Delta - Mn^{2+} + \frac{1}{2}O_2\uparrow \quad (8)$$

Figure 4b shows the O 1s XPS spectra of all samples. The surface-adsorbed oxygen species (O_2^-, O_2^{2-}, or O^-) at 529.8 eV, lattice oxygen (O_{latt}) at 531.4 eV, and carbonate (CO_3^{2-}) or hydroxide (OH^-) at 533.3 eV, respectively, appeared on the catalysts' surfaces.[11,45] The virtually indistinguishable peak showed that CO_3^{2-} or OH^- on the surface of the catalyst has been removed well in the preparation process. The O_{ads}/O_{latt} molar ratio can also indirectly show the concentration of the oxygen vacancies because O_{ads} originated from the dissociation of adsorbed O_2 on oxygen vacancies.[49] As shown in Table 1, the increase of the O_{ads}/O_{latt} ratio followed the order of Mn_3O_4 (0.47) < $Mn_{3-x}Cu_xO_4$ (0.53) < $Mn_{3-x}Fe_xO_4$, which also represented the abundance of surface oxygen vacancies.

The type and mobility of oxygen species were ascertained through temperature-programmed desorption with oxygen (O_2-TPD; Figure 4c). Considering that oxygen desorption commonly occurs below 400 °C and that above 400 °C is assigned to the release of bulk oxygen,[19] the O_2-TPD peaks of three samples below 400 °C were analyzed by curve-fitting (Figure 4d). The three peaks for Mn_3O_4 correspond to the physisorbed molecular oxygen (126 °C), the chemisorbed oxygen atoms on the surface (203 °C), and the chemisorbed oxygen atomss in the lattice layer of the surface (281 °C).[11] After doping Fe and Cu ions, the peak positions of all oxygen desorption for $Mn_{3-x}Cu_xO_4$ and $Mn_{3-x}Fe_xO_4$ shifted toward

DOI: 10.1021/acs.inorgchem.9b02105
Inorg. Chem. XXXX, XXX, XXX−XXX

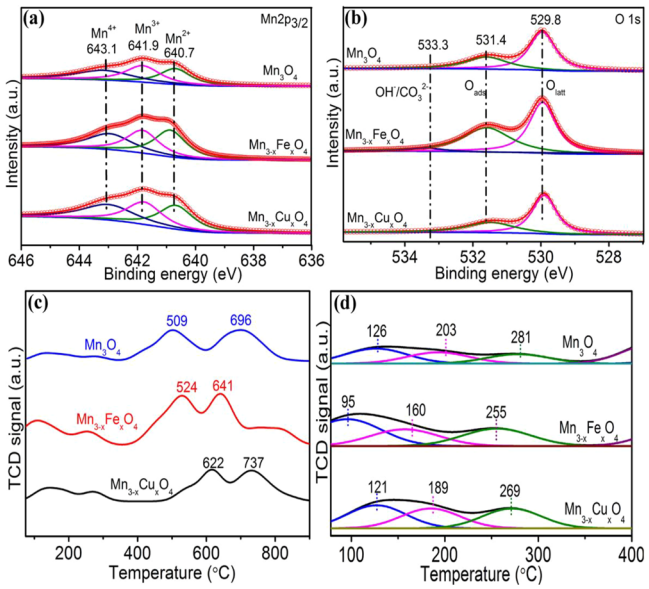

Figure 4. (a) Mn $2p_{3/2}$ XPS spectra. (b) O 1s XPS spectra. O_2-TPD profiles of Mn_3O_4, $Mn_{3-x}Fe_xO_4$, and $Mn_{3-x}Cu_xO_4$ (x = 0.6): (c) 80−900 °C; (d) 80−400 °C.

the low-temperature range, illustrating that the active oxygen could be release more readily. Moreover, $Mn_{3-x}Fe_xO_4$ possessed an oxygen desorption capacity superior to that of $Mn_{3-x}Cu_xO_4$, manifesting more surface defects in the $Mn_{3-x}Fe_xO_4$ catalyst.

Before the performance of the samples was assessed, a blank measurement was executed with no catalyst, and the removal of toluene was not found below 350 °C, indicating that, under the reaction conditions adopted, no homogeneous reaction took place.[45] Figure 5a shows the evaluation of toluene

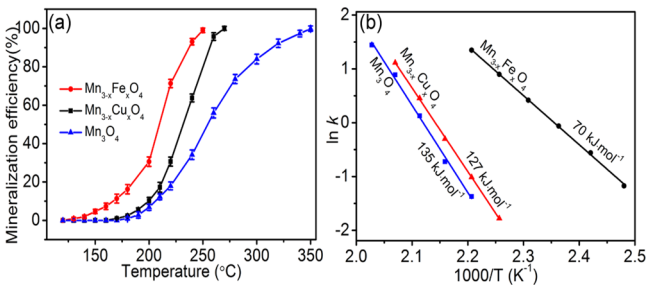

Figure 5. (a) ME of toluene. (b) Dynamic study of the behavior of catalysts in deep oxidization of toluene over Mn_3O_4, $Mn_{3-x}Cu_xO_4$, and $Mn_{3-x}Fe_xO_4$ (x = 0.6).

oxidation. Over Mn_3O_4, $Mn_{3-x}Fe_xO_4$, and $Mn_{3-x}Cu_xO_4$, the ME of toluene was enhanced with a rise in the temperature, and $Mn_{3-x}Fe_xO_4$ presented the most activity among of all of the samples. T_{50} and T_{90} (temperatures vs ME of 50 and 90%) were used to appraise the catalytic performance of three catalysts. For $Mn_{3-x}Fe_xO_4$, the values of T_{50} and T_{90} for toluene mineralization were 199 and 224 °C, which were much lower in comparison with those of $Mn_{3-x}Cu_xO_4$ (232 and 256 °C) and Mn_3O_4 (255 and 315 °C), showing that $Mn_{3-x}Fe_xO_4$ possesses a lower light-off temperature. Generally, catalytic oxidation of the VOC at low reaction temperature is affected by the O_{ads} concentration and specific surface area.[11,19,45,51,52] Combined with the above various characterizations, it can be discovered that the pure Mn_3O_4 has a relatively low number of oxygen vacancies and low surface areas (Table 1), and this was detrimental to the O_{ads} generation and contact between the catalyst and VOC to some extent. However, when Fe and Cu were added into the system, the acquired $Mn_{3-x}Fe_xO_4$ and $Cu_xMn_{3-x}O_4$ held a higher proportion of O_{ads} and a larger specific surface area, thus bringing better activity in comparison with that of Mn_3O_4. In addition, the complete incorporation of Fe into Mn_3O_4 crystals can cause more crystal defects, thereby greatly increasing the oxygen vacancy concentration and further enhancing the active species of catalysts. This promotes a higher catalytic activity of $Mn_{3-x}Fe_xO_4$ compared to $Mn_{3-x}Cu_xO_4$.

In order to explore the intrinsic characteristics of catalysts, we herein introduced the apparent activation energy, which can exclude the effect of specific surface area.[19] The E_a values of toluene mineralization (Figure 5b) increased in the order of $Mn_{3-x}Fe_xO_4$ (70 kJ·mol^{-1}) < $Mn_{3-x}Cu_xO_4$ (127 kJ·mol^{-1}) < Mn_3O_4 (135 kJ·mol^{-1}), suggesting that $Mn_{3-x}Fe_xO_4$ has the highest surface oxygen species, which were also easier to release, allowing toluene to be more susceptible to deep oxidation over $Mn_{3-x}Fe_xO_4$-0.6. Moreover, the E_a value over $Mn_{3-x}Fe_xO_4$-0.6 (70 kJ·mol^{-1}) was also much lower than those of Mn−Fe oxide (127.2 kJ·mol^{-1}; deep oxidation),[18] MnO_2 (153.0 kJ·mol^{-1}; deep oxidation),[18] CeO_2 (90.9 kJ·mol^{-1}; deep oxidation),[17] Mn−Ce oxide (88.1 kJ·mol^{-1}; deep oxidation),[17] $Cu_{1.5}Mn_{1.5}O_4$ (111.2 kJ·mol^{-1}; total oxidation),[53] MnO/CeO_2 (>127.6 kJ·mol^{-1}; total oxidation),[54] MnO_x/Al_2O_3 (133.0 kJ·mol^{-1}; total oxidation),[54] and $Ni_{0.5}Zn_{0.5}Fe_2O_4$ (94 kJ·mol^{-1}; total oxidation).[55] Generally, the activity of catalysts was decided by their structures, metal states, and redox properties, which can be increased by an optimized preparation method.[18,56] Therefore, we reckoned that the distinction between the E_a value over $Mn_{3-x}Fe_xO_4$ and the literature values should be ascribed to a high oxygen vacancy concentration in $Mn_{3-x}Fe_xO_4$. According to the above test results, the influence of the internal and external mass diffusion on the catalytic reaction rate of toluene oxidation can be excluded (Figure S6).

The reducibility of samples with different contents of Fe evaluated by H_2-TPR is displayed in Figure 6a,b and listed in

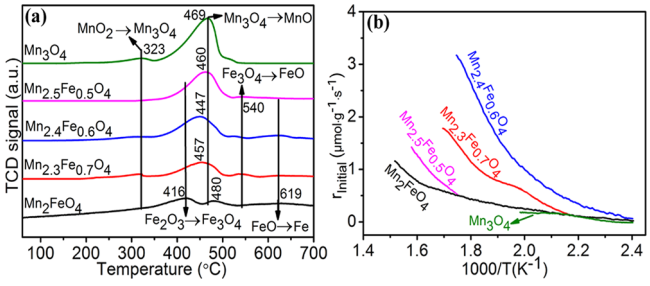

Figure 6. (a) H_2-TPR profiles and (b) initial H_2 consumption rates at low temperature of $Mn_{3-x}Fe_xO_4$ with various amounts of Fe.

Table 2. The peaks of Mn_3O_4 at 323 and 469 °C were due to the conversion of MnO_2 to Mn_3O_4 and Mn_3O_4 to MnO, respectively.[27] After Fe was incorporated into Mn_3O_4, the peak belonging to the conversion of Mn_3O_4 to MnO shifted obviously, and it appeared at 460 °C for $Mn_{2.5}Fe_{0.5}O_4$, 447 °C for $Mn_{2.4}Fe_{0.6}O_4$, 457 °C for $Mn_{2.3}Fe_{0.7}O_4$, and 480 °C for Mn_2FeO_4, respectively. Also, the reduction temperature tends to decrease first and then increase gradually with an increase of

DOI: 10.1021/acs.inorgchem.9b02105
Inorg. Chem. XXXX, XXX, XXX−XXX

Table 2. H_2 Consumption, O_2 Uptake, Metal Dispersion, and TOF of $Mn_{2.4}Fe_{0.6}O_4$

sample	ICP-Mn (wt %)	total H_2 uptake (μmol·g_{cat}^{-1})	O_2 uptake at 350 °C (μmol·g_{cat}^{-1})	Mn dispersion[a] (%)	TOF at 160 °C (10^{-6} s^{-1})
Mn_3O_4	72.3	3785	17299	33	0.05
$Mn_{2.5}Fe_{0.5}O_4$	59.8	4581	18266	42	3.53
$Mn_{2.4}Fe_{0.6}O_4$	57.2	5067	23296	56	6.52
$Mn_{2.3}Fe_{0.7}O_4$	54.5	5359	19025	48	5.81
Mn_2FeO_4	47.8	5991	13558	39	1.23
γ-Fe_2O_3	0	11648	0	0	0

[a]Mn dispersion: fraction of Mn atoms at the catalyst surface.

the iron content. The incorporation of a small number of Fe ions led to a loose lattice of Mn_3O_4, which was favorable for the contact of Mn^{3+} with H_2. Furthermore, it can be also seen that the peaks at 416, 540, and 619 °C for Mn_2FeO_4 were assigned to the conversion of Fe_2O_3 to Fe_3O_4, Fe_3O_4 to FeO, and FeO to Fe.[18,27] Namely, Fe_2O_3 was first reduced to Fe_3O_4 before Mn_3O_4 was reduced to MnO. Therefore, the addition of excessive Fe into Mn_3O_4 resulted in more Fe_3O_4 oxide films on the catalysts' surfaces during the reduction process, which delayed the normal reduction of Mn^{3+}. Besides, the total H_2 consumption of $Mn_{3-x}Fe_xO_4$ was improved in comparison with Mn_3O_4 because Fe^{3+} was finally reduced to Fe^0. The total H_2 consumption increased in the order of Mn_3O_4 < $Mn_{2.5}Fe_{0.5}O_4$ < $Mn_{2.4}Fe_{0.6}O_4$ < $Mn_{0.3}Fe_{0.7}O_4$ < Mn_2FeO_4 < γ-Fe_2O_3 (Table 2). Moreover, the reducibility of catalysts was evaluated by an initial H_2 uptake rate at low temperature (Figure 6b). The reducibility at low temperature was decreased in the proper order of $Mn_{2.4}Fe_{0.6}O_4$ > $Mn_{2.3}Fe_{0.7}O_4$ > $Mn_{2.5}Fe_{0.5}O_4$ > Mn_2FeO_4 > Mn_3O_4, suggesting that $Mn_{2.4}Fe_{0.6}O_4$ has more oxygen vacancies and surface active oxygen atoms as well as better catalytic activity.

In addition, it should be noted that only active metals were considered to play major roles in VOC oxidation rather than all metal ions of catalysts. Therefore, the dispersion of surface Mn of $Mn_{3-x}Fe_xO_4$ is necessary for evaluation. According to the H_2-TPR results and considering the fact that these samples were synthesized at a relatively low temperature and their performance was tested below 350 °C (Figure S7), we herein selected 350 °C as the oxygen pulse chemisorption temperature.[57] The O_2 uptake of catalysts at 350 °C is listed in Table 2. The dispersion of surface Mn of $Mn_{2.4}Fe_{0.6}O_4$ (56%) was higher than those of Mn_3O_4 (33%), $Mn_{2.3}Fe_{0.7}O_4$ (48%), $Mn_{2.5}Fe_{0.5}O_4$ (42%), and Mn_2FeO_4 (39%), suggesting that utilization of Mn was the highest in $Mn_{2.4}Fe_{0.6}O_4$ and a maximum number of oxygen vacancies were present in the catalyst.

The catalytic performance of various amounts of Fe doped in Mn_3O_4 was also tested for low-temperature oxidation of toluene. Because toluene oxidation occurred at the active sites of catalysts, the catalytic activities of samples were estimated by using turnover frequency (TOF). As depicted in Figure 7a, the TOF values enhanced in the sequence of Mn_3O_4 < Mn_2FeO_4 < $Mn_{2.5}Fe_{0.5}O_4$ < $Mn_{2.3}Fe_{0.7}O_4$ < $Mn_{2.4}Fe_{0.6}O_4$, which is consistent with the dispersion trend of Mn. The results showed a better catalytic performance of $Mn_{2.4}Fe_{0.6}O_4$, indicating that the suitable incorporation of Fe can play a positive role in the catalytic activity. Moreover, according to the TOF values of $Mn_{3-x}Fe_xO_4$ at 160 °C, the changes in the ratios of $(Mn^{3+} + Mn^{2+})/Mn^{4+}$ and O_{ads}/O_{latt} were also evaluated by XPS. As shown in Figure 7b, the curves of the TOF values, the ratios of $(Mn^{3+} + Mn^{2+})/Mn^{4+}$, and O_{ads}/O_{latt} with different contents of Fe displayed volcano-shaped

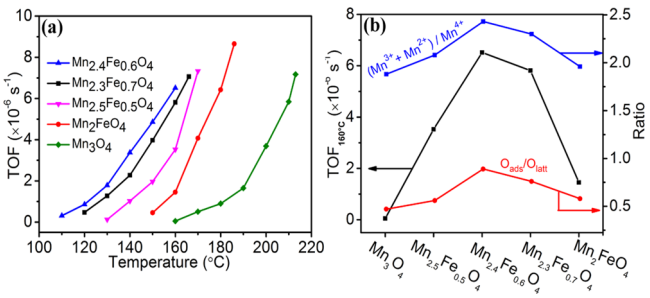

Figure 7. (a) Temperature-dependent changes of the TOF values. (b) Samples with different amounts of Fe versus TOF values at 160 °C and molar ratios of $(Mn^{3+} + Mn^{2+})/Mn^{4+}$ and O_{ads}/O_{latt}.

tendencies, demonstrating that the suitable amount of Fe incorporated could also increase the concentration of low-valence Mn and O_{ads} on the surface of catalysts, further suggesting that more oxygen vacancies were present in $Mn_{2.4}Fe_{0.6}O_4$.

Moreover, the intermediates in toluene oxidation over $Mn_{2.4}Fe_{0.6}O_4$ were also detected by in situ diffuse-reflectance infrared Fourier transform spectroscopy (DRIFTS) and gas chromatography−mass spectrometry (GC−MS). It can be observed from in situ Fourier transform infrared spectroscopy (Figure 8a) that a series of surface structural changes for

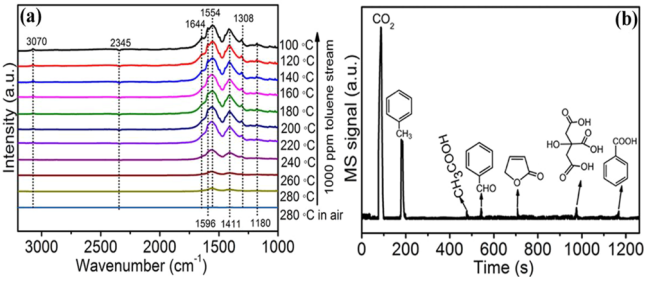

Figure 8. (a) Change of DRIFTS of $Mn_{3-x}Fe_xO_4$ for toluene oxidation, (b) GC−MS results of the exhaust gas.

$Mn_{2.4}Fe_{0.6}O_4$ have emerged. With the temperature-dependent changes, a band appears at 3070 cm^{-1}, corresponding to C−H of the vinyl stretching vibration.[58] The band at 2345 cm^{-1} was assigned to the CO_2 vibration, and the peaks at 1644 cm^{-1} were the vibration mode of −OH and the H_2O deformation vibration, respectively.[27,58] The strong bands at 1596, 1554, and 1411 cm^{-1} were due to the C−C and C═O stretching vibrations as well as carbonate species,[18,59] respectively. Moreover, the vibration modes at 1308 and 1180 cm^{-1} were according to the ν_s(COO) stretching vibration.[27] These results showed that toluene over $Mn_{2.4}Fe_{0.6}O_4$ was oxidized to −CHO, −COOH, or −COOC− organics. According to the

DOI: 10.1021/acs.inorgchem.9b02105
Inorg. Chem. XXXX, XXX, XXX−XXX

detection of exhaust gas by GC−MS (Figure 8b), it can be found that acetic acid, benzaldehyde, 2-(5*H*)-furanone, citric acid, and benzoic acid coexisted in the exhaust gas after low-temperature catalytic oxidation of toluene. Combined with DRIFTS and GC−MS characterizations, the possible degradation path of toluene undergoes the production of benzaldehyde, benzoic acid, 2-(5*H*)-furanone, citric acid, and acetic acid, further oxidation to organic salts, thus conversion to inorganic salts; ultimately, the inorganic salts decomposed to CO_2. Besides, the activated O_2 molecules can supplement the spent active oxygen over oxygen vacancies.

The catalytic stability of $Mn_{2.4}Fe_{0.6}O_4$ was also carried out under long time-on-stream conditions (120 h of uninterrupted reaction). As shown in Figure 9, the experiment can be divided

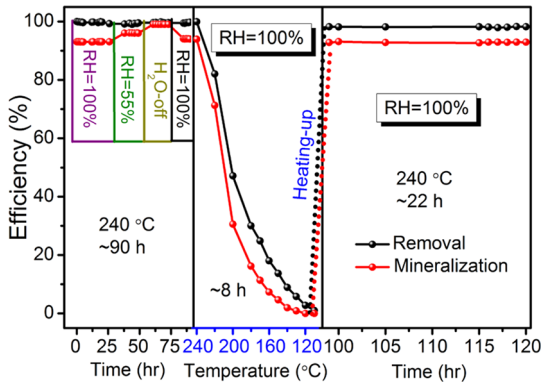

Figure 9. Catalytic stability of $Mn_{3-x}Fe_xO_4$ for the RE and ME of toluene at different humidity, 240 °C, and WHSV of 60000 mL·g^{-1}·h^{-1}.

into three stages. Obviously, the arbitrarily adjustment of the H_2O contents did not impact the RE of toluene at 240 °C for 90 h of uninterrupted reaction, except the ME of toluene. Because we know that, under heating conditions, the adsorbed oxygen was excited and overflowed from the oxygen vacancies to demineralize toluene molecules, the absorbed oxygen was supplemented by the capture and dissociation of gaseous oxygen over oxygen vacancies. Therefore, the constant flow of oxygen is necessary for the oxidation reaction to continue. During the oxidation reaction, toluene was first oxidized to benzaldehyde and benzoic acid, which consumed just a little oxygen and hardly released CO_2.[11,45] Nevertheless, the amount of oxygen trapped by the $Mn_{2.4}Fe_{0.6}O_4$ catalyst was greatly reduced by the addition of H_2O, which was made against consuming oxygen steps especially to the oxidation of intermediates including −COOH. Consequently, the added H_2O could play a distinct effect on the toluene ME compared to the RE of toluene. Following the first stage, the oxidation experiment of toluene with a decrease in the reaction temperature from 240 to 110 °C was performed (RH = 100%). The test results were similar to those of Figures 5a and S5, implying that the $Mn_{2.4}Fe_{0.6}O_4$ catalyst has good stability. Subsequently, the reaction system was quickly recovered to a constant temperature of 240 °C (RH = 100%). It is obvious that the RE and ME of toluene had also been restored. Furthermore, the activity of $Mn_{2.4}Fe_{0.6}O_4$ was still not attenuated after recycle, and the crystal structure after 120 h of reaction did not change, which can be determined by XRD (Figure S8), further suggesting that $Mn_{2.4}Fe_{0.6}O_4$ holds high stability.

4. CONCLUSION

A series of $Mn_{3-x}Fe_xO_4$ spinels with different amounts of oxygen vacancies were synthesized by regulating the insertion of Fe ions. The influence of the doping ion type and ion doping degree on the oxygen vacancy concentration and catalytic performance of catalysts was studied. The improvement of physical−chemical properties such as the structures, lattice defects, and morphologies leads to the better low-temperature activity for toluene oxidation over $Mn_{3-x}Fe_xO_4$ catalyst. For the most active $Mn_{2.4}Fe_{0.6}O_4$ catalyst, its increased performance can be due to the higher concentration of structural defect and oxygen vacancy and larger (Mn^{3+} + Mn^{2+})/Mn^{4+} and O_{ads}/O_{latt} ratios. The test under simulated realistic exhaust gas also showed that $Mn_{2.4}Fe_{0.6}O_4$ is a superior catalyst (T_{50} = 199 °C and T_{90} = 224 °C for toluene mineralization; $TOF_{160\ °C}$ = 6.52 × 10^{-6} s^{-1}) with stability (long-term toluene oxidation test running for 120 h) and satisfied endurability to high humidity (RH = 55% and 100%). With systemic dynamic research on toluene oxidation over $Mn_{2.4}Fe_{0.6}O_4$, the principles for toluene activation and CO_2 production were proven to be dissimilar. We can rationally anticipate that the $Mn_{2.4}Fe_{0.6}O_4$ spinel is an effective and promising catalyst for the removal of VOCs.

■ ASSOCIATED CONTENT

Supporting Information

The Supporting Information is available free of charge on the ACS Publications website at DOI: 10.1021/acs.inorgchem.9b02105.

Characterization, XRD patterns of γ-Fe_2O_3 and $Mn_{3-x}Fe_xO_4$ before and after catalytic reaction, EDS mapping spectrum of $Mn_{3-x}Cu_xO_4$ and $Mn_{3-x}Fe_xO_4$, Cu 2p XPS spectra of $Mn_{3-x}Cu_xO_4$, RE of toluene over $Mn_{3-x}Fe_xO_4$, $Mn_{3-x}Cu_xO_4$, and Mn_3O_4, effect of the WHSV on toluene mineralization, and RE of toluene over samples with different contents of Fe (PDF)

■ AUTHOR INFORMATION

Corresponding Authors

*E-mail: Lzliu@ntu.edu.cn (L.L.).

*E-mail: sunth@sjtu.edu.cn (T.S.).

ORCID

Lizhong Liu: 0000-0002-6171-8513

Tonghua Sun: 0000-0003-3803-0232

Jinping Jia: 0000-0003-2409-338X

Notes

The authors declare no competing financial interest.

■ ACKNOWLEDGMENTS

The authors are grateful for financial support from the National Natural Science Foundation of China (Grant 21876107).

■ REFERENCES

(1) Zhou, H.; Wen, Z.; Liu, J.; Ke, J.; Duan, X.; Wang, S. Z-scheme plasmonic Ag decorated WO_3/Bi_2WO_6 hybrids for enhanced photocatalytic abatement of chlorinated-VOCs under solar light irradiation. *Appl. Catal., B* **2019**, *242*, 76−84.

(2) Hu, F.; Peng, Y.; Chen, J.; Liu, S.; Song, H.; Li, J. Low content of CoO_x supported on nanocrystalline CeO_2 for toluene combustion: The importance of interfaces between active sites and supports. *Appl. Catal., B* **2019**, *240*, 329−336.

DOI: 10.1021/acs.inorgchem.9b02105
Inorg. Chem. XXXX, XXX, XXX−XXX

(3) Li, J. J.; Yu, E. Q.; Cai, S. C.; Chen, X.; Chen, J.; Jia, H. P.; Xu, Y. J. Noble metal free, $CeO_2/LaMnO_3$ hybrid achieving efficient photothermal catalytic decomposition of volatile organic compounds under IR light. *Appl. Catal., B* **2019**, *240*, 141−152.
(4) Yan, Q.; Li, X.; Zhao, Q.; Chen, G. Shape-controlled fabrication of the porous Co_3O_4 nanoflower clusters for efficient catalytic oxidation of gaseous toluene. *J. Hazard. Mater.* **2012**, *209*−*210*, 385−391.
(5) Everaert, K.; Baeyens, J. Catalytic combustion of volatile organic compounds. *J. Hazard. Mater.* **2004**, *109*, 113−139.
(6) Ye, Z.; Giraudon, J. M.; Nuns, N.; Simon, P.; De Geyter, N.; Morent, R.; Lamonier, J. F. Influence of the preparation method on the activity of copper-manganese oxides for toluene total oxidation. *Appl. Catal., B* **2018**, *223*, 154−166.
(7) Vildozo, D.; Portela, R.; Ferronato, C.; Chovelon, J.-M. Photocatalytic oxidation of 2-propanol/toluene binary mixtures at indoor air concentration levels. *Appl. Catal., B* **2011**, *107*, 347−354.
(8) Su, Y.; Zhang, X.; Wei, X. M.; Kong, J. Y.; Xia, F. F.; Li, W.; He, R. Evaluation of simultaneous biodegradation of methane and toluene in landfill covers. *J. Hazard. Mater.* **2014**, *274*, 367−375.
(9) Obuskovic, G.; Majumdar, S.; Sirkar, K. K. Highly VOC-selective hollow fiber membranes for separation by vapor permeation. *J. Membr. Sci.* **2003**, *217*, 99−116.
(10) Chang, T.; Shen, Z.; Huang, Y.; Lu, J.; Ren, D.; Sun, J.; Cao, J.; Liu, H. Post-plasma-catalytic removal of toluene using MnO_2−Co_3O_4 catalysts and their synergistic mechanism. *Chem. Eng. J.* **2018**, *348*, 15−25.
(11) Liu, L.; Li, J.; Zhang, H.; Li, L.; Zhou, P.; Meng, X.; Guo, M.; Jia, J.; Sun, T. In situ fabrication of highly active γ-$MnO_2/SmMnO_3$ catalyst for deep catalytic oxidation of gaseous benzene, ethylbenzene, toluene, and o-xylene. *J. Hazard. Mater.* **2019**, *362*, 178−186.
(12) Peng, R.; Sun, X.; Li, S.; Chen, L.; Fu, M.; Wu, J.; Ye, D. Shape effect of Pt/CeO_2 catalysts on the catalytic oxidation of toluene. *Chem. Eng. J.* **2016**, *306*, 1234−1246.
(13) Mei, J.; Qu, Z.; Zhao, S.; Hu, X.; Xu, H.; Yan, N. Promoting effect of Mn and Ti on the structure and performance of Co_3O_4 catalysts for oxidation of dibromomethane. *J. Ind. Eng. Chem.* **2018**, *57*, 208−215.
(14) Mei, J.; Wang, C.; Kong, L.; Liu, X.; Hu, Q.; Zhao, H.; Yang, S. Outstanding performance of recyclable amorphous MoS_3 supported on TiO_2 for capturing high concentrations of gaseous elemental mercury: Mechanism, kinetics, and application. *Environ. Sci. Technol.* **2019**, *53*, 4480−4489.
(15) Mei, J.; Zhao, S.; Huang, W.; Qu, Z.; Yan, N. Mn-Promoted Co_3O_4/TiO_2 as an efficient catalyst for catalytic oxidation of dibromomethane (CH_2Br_2). *J. Hazard. Mater.* **2016**, *318*, 1−8.
(16) Mei, J.; Ke, Y.; Yu, Z.; Hu, X.; Qu, Z.; Yan, N. Morphology-dependent properties of Co_3O_4/CeO_2 catalysts for low temperature dibromomethane (CH_2Br_2) oxidation. *Chem. Eng. J.* **2017**, *320*, 124−134.
(17) Chen, J.; Chen, X.; Chen, X.; Xu, W.; Xu, Z.; Jia, H.; Chen, J. Homogeneous introduction of CeO_y into MnO_x-based catalyst for oxidation of aromatic VOCs. *Appl. Catal., B* **2018**, *224*, 825−835.
(18) Chen, J.; Chen, X.; Xu, W.; Xu, Z.; Chen, J.; Jia, H.; Chen, J. Hydrolysis driving redox reaction to synthesize Mn-Fe binary oxides as highly active catalysts for the removal of toluene. *Chem. Eng. J.* **2017**, *330*, 281−293.
(19) Si, W.; Wang, Y.; Zhao, S.; Hu, F.; Li, J. A facile method for in situ preparation of the $MnO_2/LaMnO_3$ catalyst for the removal of toluene. *Environ. Sci. Technol.* **2016**, *50*, 4572−4578.
(20) Li, W. B.; Wang, J. X.; Gong, H. Catalytic combustion of VOCs on non-noble metal catalysts. *Catal. Today* **2009**, *148*, 81−87.
(21) Jiang, S.; Song, S. Enhancing the performance of Co_3O_4/CNTs for the catalytic combustion of toluene by tuning the surface structures of CNTs. *Appl. Catal., B* **2013**, *140*−*141*, 1−8.
(22) Rokicińska, A.; Natkański, P.; Dudek, B.; Drozdek, M.; Lityńska-Dobrzyńska, L.; Kuśtrowski, P. Co_3O_4-pillared montmorillonite catalysts synthesized by hydrogel-assisted route for total oxidation of toluene. *Appl. Catal., B* **2016**, *195*, 59−68.
(23) Santos, V. P.; Pereira, M. F. R.; Órfão, J. J. M.; Figueiredo, J. L. The role of lattice oxygen on the activity of manganese oxides towards the oxidation of volatile organic compounds. *Appl. Catal., B* **2010**, *99*, 353−363.
(24) Kim, S. C.; Shim, W. G. Catalytic combustion of VOCs over a series of manganese oxide catalysts. *Appl. Catal., B* **2010**, *98*, 180−185.
(25) Piumetti, M.; Fino, D.; Russo, N. Mesoporous manganese oxides prepared by solution combustion synthesis as catalysts for the total oxidation of VOCs. *Appl. Catal., B* **2015**, *163*, 277−287.
(26) Huang, H.; Xu, Y.; Feng, Q.; Leung, D. Y. C. Low temperature catalytic oxidation of volatile organic compounds: a review. *Catal. Sci. Technol.* **2015**, *5*, 2649−2669.
(27) Pan, H.; Jian, Y.; Chen, C.; He, C.; Hao, Z.; Shen, Z.; Liu, H. Sphere-shaped Mn_3O_4 catalyst with remarkable low-temperature activity for methyl−ethyl−ketone combustion. *Environ. Sci. Technol.* **2017**, *51*, 6288−6297.
(28) Tomatis, M.; Xu, H. H.; He, J.; Zhang, X. D. Recent development of catalysts for removal of volatile organic compounds in flue gas by combustion: a review. *J. Chem.* **2016**, *2016*, 1−15.
(29) Shangguan, W. F.; Teraoka, Y.; Kagawa, S. Simultaneous catalytic removal of NO_χ and diesel soot particulates over ternary AB_2O_4 spinel-type oxides. *Appl. Catal., B* **1996**, *8*, 217−227.
(30) Hammiche-Bellal, Y.; Benadda, A.; Meddour-Boukhobza, L.; Barama, S.; Djadoun, A.; Barama, A. Preparation and catalytic activity in ethanol combustion reaction of cobalt−iron spinel catalysts. *Catal. Commun.* **2013**, *42*, 62−67.
(31) Behar, S.; Gonzalez, P.; Agulhon, P.; Quignard, F.; Świerczyński, D. New synthesis of nanosized Cu−Mn spinels as efficient oxidation catalysts. *Catal. Today* **2012**, *189*, 35−41.
(32) Castaño, M. H.; Molina, R.; Moreno, S. Catalytic oxidation of VOCs on $MnMgAlO_x$ mixed oxides obtained by auto-combustion. *J. Mol. Catal. A: Chem.* **2015**, *398*, 358−367.
(33) Jia, J.; Yang, W.; Zhang, P.; Zhang, J. Facile synthesis of Fe-modified manganese oxide with high content of oxygen vacancies for efficient airborne ozone destruction. *Appl. Catal., A* **2017**, *546*, 79−86.
(34) Suárez-Vázquez, S. I.; Gil, S.; García-Vargas, J. M.; Cruz-López, A.; Giroir-Fendler, A. Catalytic oxidation of toluene by $SrTi_{1-X}B_XO_3$ (B = Cu and Mn) with dendritic morphology synthesized by one pot hydrothermal route. *Appl. Catal., B* **2018**, *223*, 201−208.
(35) Maurer, M.; Ravet, M. F.; Ousset, J. C.; Gourteux, T.; Fontaine, A.; Tolentino, H.; Dartyge, E.; Tourillon, G.; Krill, G.; Kes, P. H. Electronic structure of Y $Ba_2Cu_3O_{7-\delta}$ ceramics as a function of δ: Homogeneous mixed valent state and superconductivity. *Phys. C* **1988**, *153*, 145−146.
(36) Zhang, L.; Zhang, Y.; Dai, H.; Deng, J.; Wei, L.; He, H. Hydrothermal synthesis and catalytic performance of single-crystalline $La_{2-x}Sr_xCuO_4$ for methane oxidation. *Catal. Today* **2010**, *153*, 143−149.
(37) Yuan, J.; Dai, H.; Zhang, L.; Deng, J.; Liu, Y.; Zhang, H.; Jiang, H.; He, H. PMMA-templating preparation and catalytic properties of high-surface-area three-dimensional macroporous La_2CuO_4 for methane combustion. *Catal. Today* **2011**, *175*, 209−215.
(38) Dou, S. X.; Liu, H. K.; Bourdillon, A. J.; Tan, N. X.; Savvides, N.; Zhou, J. P.; Sorrell, C. C. Labile Cu^{3+} ions in the Bi-Sr-Ca-Cu-O system and the effects of varying the composition and heat treatment. *Supercond. Sci. Technol.* **1988**, *1*, 78−82.
(39) Su, M. Y.; Dorris, S. E.; Mason, T. O. Defect model and transport at high temperature in $YBa_2Cu_3O_{6+\gamma}$. *J. Solid State Chem.* **1988**, *75*, 381−389.
(40) Blumberg, W. E.; Eisinger, J.; Geschwind, S. Cu^{3+} ion in Corundum. *Phys. Rev.* **1963**, *130*, 900−909.
(41) Marbán, G.; Fuertes, A. B. Highly active and selective CuO_x/CeO_2 catalyst prepared by a single-step citrate method for preferential oxidation of carbon monoxide. *Appl. Catal., B* **2005**, *57*, 43−53.
(42) Kim, M.; Chen, X. M.; Wang, X.; Nelson, C. S.; Budakian, R.; Abbamonte, P.; Cooper, S. L. Pressure- and field-tuning the magnetostructural phases of Mn_3O_4: Raman scattering and X-ray

DOI: 10.1021/acs.inorgchem.9b02105
Inorg. Chem. XXXX, XXX, XXX−XXX

diffraction studies. *Phys. Rev. B: Condens. Matter Mater. Phys.* **2011**, *84*, 3239−3247.
(43) Malavasi, L.; Galinetto, P.; Mozzati, M. C.; Azzoni, C. B.; Flor, G. Raman spectroscopy of AMn_2O_4 (A = Mn, Mg and Zn) spinels. *Phys. Chem. Chem. Phys.* **2002**, *4*, 3876−3880.
(44) Osswald, S.; Mochalin, V. N.; Havel, M.; Yushin, G.; Gogotsi, Y. Phonon confinement effects in the Raman spectrum of nanodiamond. *Phys. Rev. B: Condens. Matter Mater. Phys.* **2009**, *80* (7), 75419.
(45) Liu, L.; Zhang, H.; Jia, J.; Sun, T.; Sun, M. Direct Molten Polymerization Synthesis of Highly Active Samarium Manganese Perovskites with Different Morphologies for VOC Removal. *Inorg. Chem.* **2018**, *57*, 8451−8457.
(46) Nayak, N. B.; Nayak, B. B. Temperature-mediated phase transformation, pore geometry and pore hysteresis transformation of borohydride derived in-born porous zirconium hydroxide nanopowders. *Sci. Rep.* **2016**, *6*, 26404−26413.
(47) Ding, J.; Liu, L.; Xue, J.; Zhou, Z.; He, G.; Chen, H. Low-temperature preparation of magnetically separable Fe_3O_4@CuO-RGO core-shell heterojunctions for high-performance removal of organic dye under visible light. *J. Alloys Compd.* **2016**, *688*, 649−656.
(48) Si, W.; Wang, Y.; Peng, Y.; Li, J. Selective dissolution of A-site cations in ABO_3 perovskites: A new path to high-performance catalysts. *Angew. Chem., Int. Ed.* **2015**, *54*, 7954−7957.
(49) Yang, Y.; Zhang, S.; Wang, S.; Zhang, K.; Wang, H.; Huang, J.; Deng, S.; Wang, B.; Wang, Y.; Yu, G. Ball milling synthesized MnO_x as highly active catalyst for gaseous POPs removal: significance of mechanochemically induced oxygen vacancies. *Environ. Sci. Technol.* **2015**, *49*, 4473−80.
(50) Ma, Y.; Wang, R.; Wang, H.; Key, J.; Ji, S. Control of MnO_2 nanocrystal shape from tremella to nanobelt for ehancement of the oxygen reduction reaction activity. *J. Power Sources* **2015**, *280*, 526−532.
(51) Liu, L.; Jia, J.; Sun, T.; Zhang, H. A facile method for scalable preparation of mesoporous structured $SmMnO_3$ perovskites sheets for efficient catalytic oxidation of toluene. *Mater. Lett.* **2018**, *212*, 107−110.
(52) Liu, Y.; Dai, H.; Deng, J.; Zhang, L.; Zhao, Z.; Li, X.; Wang, Y.; Xie, S.; Yang, H.; Guo, G. Controlled generation of uniform spherical $LaMnO_3$, $LaCoO_3$, Mn_2O_3, and Co_3O_4 nanoparticles and their high catalytic performance for carbon monoxide and toluene oxidation. *Inorg. Chem.* **2013**, *52*, 8665−8676.
(53) Behar, S.; Gómez-Mendoza, N. A.; Gómez-García, M.Á.; Świerczyński, D.; Quignard, F.; Tanchoux, N. Study and modelling of kinetics of the oxidation of VOC catalyzed by nanosized Cu−Mn spinels prepared via an alginate route. *Appl. Catal., A* **2015**, *504*, 203−210.
(54) Saqer, S. M.; Kondarides, D. I.; Verykios, X. E. Catalytic oxidation of toluene over binary mixtures of copper, manganese and cerium oxides supported on γ-Al_2O_3. *Appl. Catal., B* **2011**, *103*, 275−286.
(55) Florea, M.; Alifanti, M.; Parvulescu, V. I.; Mihaila-Tarabasanu, D.; Diamandescu, L.; Feder, M.; Negrila, C.; Frunza, L. Total oxidation of toluene on ferrite-type catalysts. *Catal. Today* **2009**, *141*, 361−366.
(56) Zhou, G.; He, X.; Liu, S.; Xie, H.; Fu, M. Phenyl VOCs catalytic combustion on supported CoMn/AC oxide catalyst. *J. Ind. Eng. Chem.* **2015**, *21*, 932−941.
(57) Ettireddy, P. R.; Ettireddy, N.; Mamedov, S.; Boolchand, P.; Smirniotis, P. G. Surface characterization studies of TiO_2 supported manganese oxide catalysts for low temperature SCR of NO with NH_3. *Appl. Catal., B* **2007**, *76*, 123−134.
(58) Li, X.; Zhu, Z.; Zhao, Q.; Wang, L. Photocatalytic degradation of gaseous toluene over $ZnAl_2O_4$ prepared by different methods: A comparative study. *J. Hazard. Mater.* **2011**, *186*, 2089−2096.
(59) Gao, J.; Tong, X.; Li, X.; Miao, H.; Xu, J. The efficient liquid-phase oxidation of aromatic hydrocarbons by molecular oxygen in the presence of $MnCO_3$. *J. Chem. Technol. Biotechnol.* **2007**, *82*, 620−625.

DOI: 10.1021/acs.inorgchem.9b02105
Inorg. Chem. XXXX, XXX, XXX−XXX